

Impact of High-Performance Computing on New Product Design: A Case Study for a Novel Cooling System

Thomas P. Gielda

Caitin Inc, Fremont CA 94538

Email: tgielda@caitin.com

Abstract. High-performance computing has become a key enabler to fully utilize the capabilities of systems engineering. This paper describes how simulation-based design, enabled by high-performance computing, is being used to develop a novel cooling system. This study begins by developing the architecture of the novel cooling system. Next, we look at the underlying physics and the requirements of the numerical models to simulate system performance. We then look at how simulation is utilized to optimize the system architecture, and we identify critical parameters of the design.

1. Introduction

Computer-aided engineering (CAE) has become more firmly embedded in the design process. A key enabler to this embedment has been the advance in high-performance computing (HPC). Never before have we been able to visualize the performance of our devices with the fine granularity available today. The result is the ability to optimize our designs and quickly identify all the potential system/subsystem interactions of the platform. In essence, we are performing true systems engineering via simulation-based design.

This methodology can provide detailed information of system, subsystem, and component interactions. Identifying these interactions early in the design process greatly increases the probability of success when launching a new product. Failure to identify these interactions can, at best, result in program delays; at worst, they will be the cause of catastrophic failures.

Utilization of analysis tools that simulate the complete platform is critical. In this paper, we present a case study that demonstrates how high-fidelity simulation on large, parallel compute facilities can enable the innovation of new products in a virtual environment. We also study the limitations of current analytical models and develop experimental test programs that provide critical data to improve the usability of our analysis codes. The following section demonstrates how HPC was applied to develop a high-efficiency cooling system.

Case Study: Innovation of Novel Cooling Technology with HPC

In 2009, Caitin started down the path to develop a cooling system based on a new thermodynamic cycle. The Caitin cycle has inherent benefits such as the following:

1. Ability to use green refrigerants (including water)
2. Simplified system
3. Lower acquisition price

4. Represents a fundamental shift in cooling technology

In the following sections, we present the system thermodynamics of the new cycle. We then develop numerical models of the system performance of the new cycle. The numerical models are solved on HPC computers and the results then used to optimize the system design performance.

2. System Thermodynamics

Figure 1 depicts the pressure-enthalpy (p-h) diagram for a traditional vapor compression system [1].

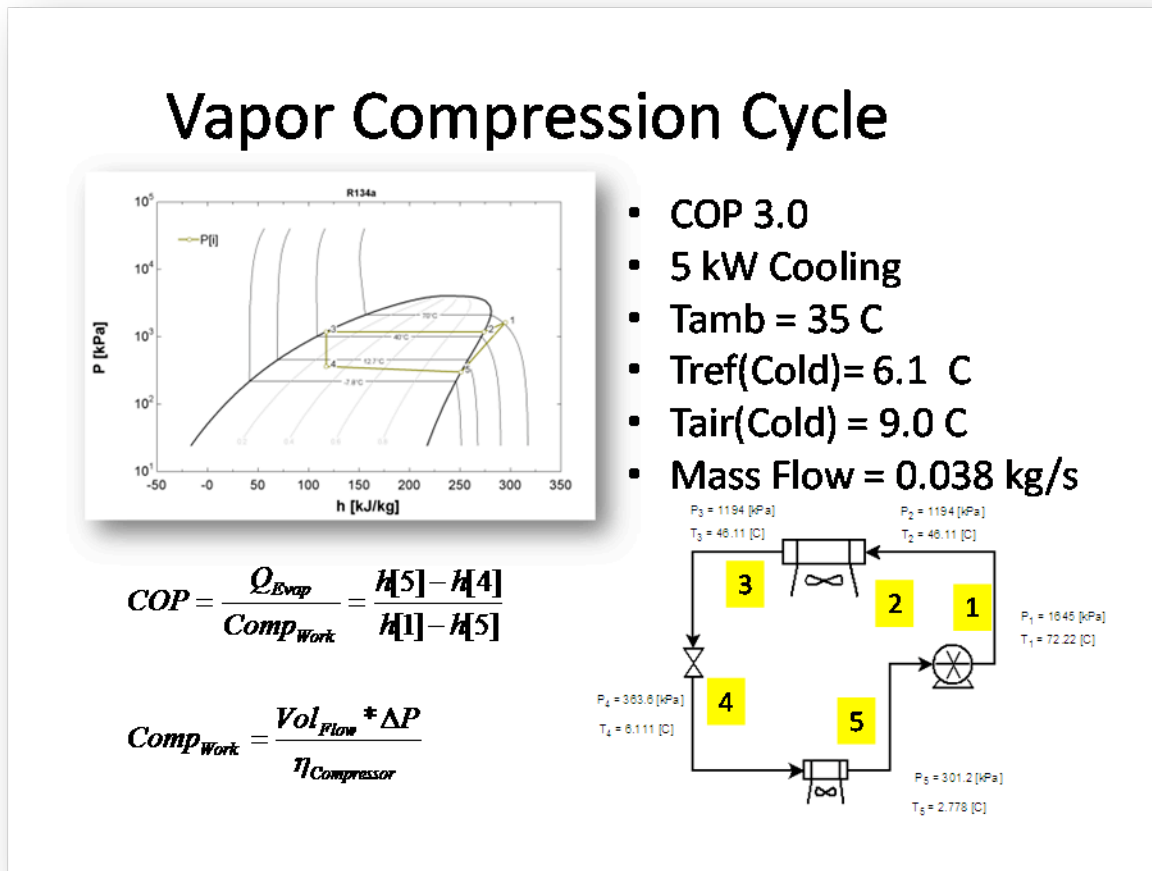


Figure 1. P-h diagram for a traditional R134a vapor compression refrigeration system.

The p-h diagram above is taken from test data for an automotive system. The overall COP of the system was approximately 3.0. For this traditional system, the compressor utilizes approximately 1.6 kW to compress the low-pressure gas (point 5 to point 1).

Caitin Cycle

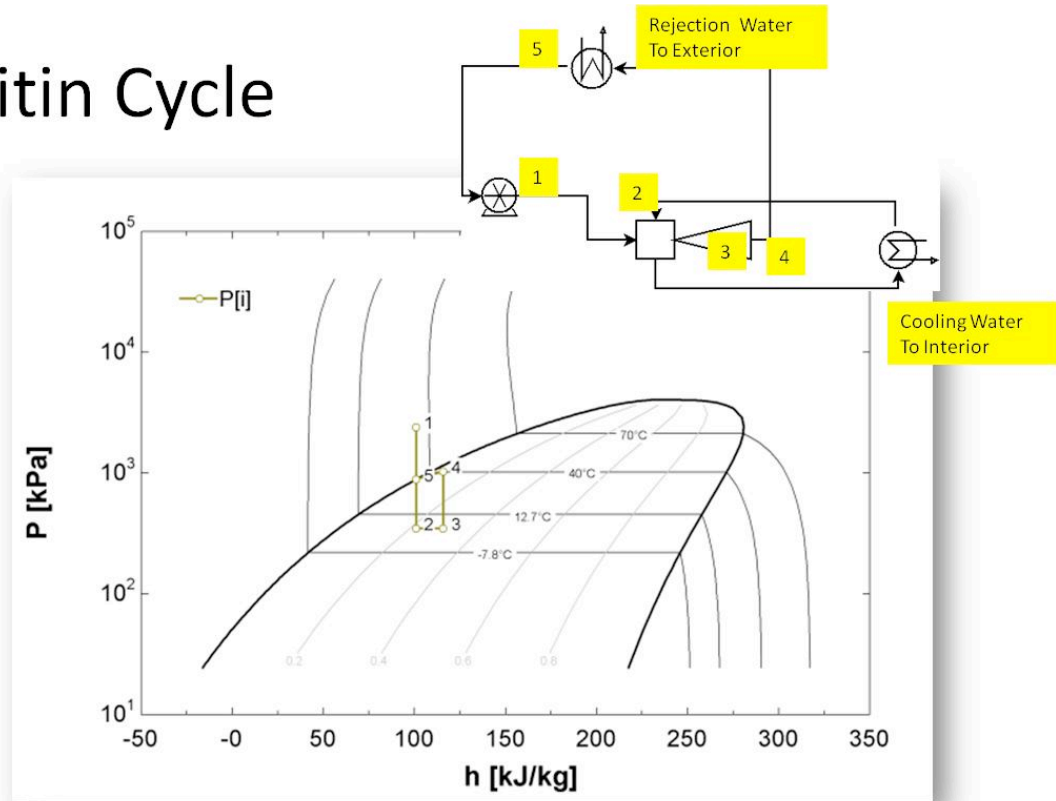


Figure 2. P-h diagram for Caitin cooling cycle.

Figure 2 depicts the p-h diagram for the Caitin cycle. A summary of the Caitin Cycle follows:

1. In Steps 1 to 2, high-pressure refrigerant undergoes an isenthalpic expansion to a point below the liquid vapor line. The efficiency of the system is determined by how far we can drive the fluid into nonequilibrium.
2. Steps 2 to 3 represent the place where the flow is accelerated down a diverging channel. This acceleration can occur only in a diverging channel when the flow is in the supersonic/hypersonic regime. In this region, the heat load is transferred to the refrigerant.
3. In Steps 3 to 4, the liquid passes through a normal shock and subsequently condenses. Since the nozzle is operating in the overexpanded regime, the shock wave is required to match the exit pressure.
4. Steps 4 to 5 depict the process in which the heat is removed from the refrigerant.
5. Steps 5 to 1 represent the pressurization of the fluid.

The pump work, Steps 5 to 1, is significantly smaller than a vapor compression system because of the greatly decreased volumetric flow rates. The pressure rise across the pump is similar to a vapor compression (VC) system. The pump work required by the Caitin cycle is

an order of magnitude less than that required by a VC system. However, since the Caitin cycle operates at reduced quality levels, our mass flow rate is significantly higher. The net result is a substantial drop in pumping power.

An important feature of the Caitin cycle is the “natural” condensation process. The shock induced condensation process can be clearly observed in Figure 3.

Condensation Shock

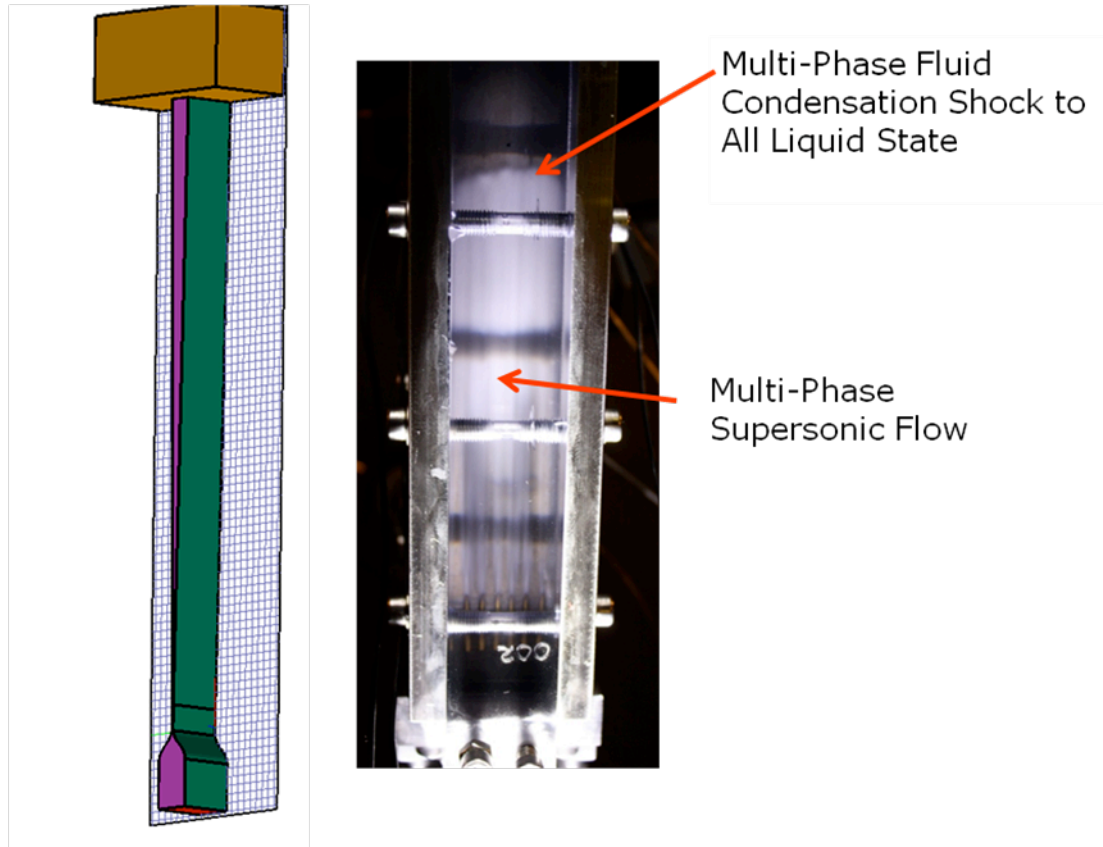


Figure 3. Visualization of the condensation shock. Water-based system: inlet pressure, 6 bar; back pressure, 1 bar. The nozzle geometry is shown on the left.

3. Numerical Analysis

Analysis of the Caitin cycle requires state-of-the-art computational fluid dynamics software. In addition, the tools must include multiphase chemically reacting flow models, including free surfaces. Figure 4 depicts the numerical models required to analyze this system.

Governing Equations

$$\iiint_{Liquid} \frac{\partial \bar{Q}_L}{\partial t} dV_{Liquid} + \iint_{Liquid} \bar{N}_L \cdot \hat{n} dA_{Liquid} = \iiint_{Liquid} \bar{H}_L dV_{Liquid}$$

$$\iiint_{Vapor} \frac{\partial \bar{Q}_V}{\partial t} dV_{Vapor} + \iint_{Vapor} \bar{N}_V \cdot \hat{n} dA_{Vapor} = \iiint_{Vapor} \bar{H}_V dV_{Vapor}$$

| | | | | |
|--------------------|---------|---|---|---|
| $\bar{Q} =$ | ρ | ρu | ρv | ρw |
| ρu | $N_x =$ | $\rho u^2 + P - \tau_{xx}$ | $N_y =$ | $\rho uv - \tau_{xy}$ |
| ρv | | $\rho uv - \tau_{xy}$ | $\rho v^2 + P - \tau_{yy}$ | $N_z =$ |
| ρw | | $\rho uw - \tau_{xz}$ | $\rho vw - \tau_{yz}$ | $\rho vw - \tau_{yz}$ |
| ρe | | $\rho uw - \tau_{xz}$ | $\rho vw - \tau_{yz}$ | $\rho w^2 + P - \tau_{zz}$ |
| ρk | | $(\rho e + P)u - u\tau_{xx} - v\tau_{xy} - w\tau_{xz} + \dot{q}_x$ | $(\rho e + P)v - u\tau_{xy} - v\tau_{yy} - w\tau_{yz} + \dot{q}_y$ | $(\rho e + P)w - u\tau_{xz} - v\tau_{yz} - w\tau_{zz} + \dot{q}_z$ |
| $\rho \varepsilon$ | | $\rho uk - \mu_k \frac{\partial k}{\partial x}$ | $\rho vk - \mu_k \frac{\partial k}{\partial y}$ | $\rho wk - \mu_k \frac{\partial k}{\partial z}$ |
| | | $\rho u\varepsilon - \mu_\varepsilon \frac{\partial \varepsilon}{\partial x}$ | $\rho v\varepsilon - \mu_\varepsilon \frac{\partial \varepsilon}{\partial y}$ | $\rho w\varepsilon - \mu_\varepsilon \frac{\partial \varepsilon}{\partial z}$ |

$$\bar{H} = \begin{matrix} \dot{m} \\ Interfacial_Force_x \\ Interfacial_Force_y \\ Interfacial_Force_z \\ \dot{m}h_g + Interfacial_Energy_Transfer \\ S_k \\ S_\varepsilon \end{matrix}$$

Figure 4. Governing equations.

From Figure 4, it becomes immediately apparent how complex this flow is. Included in the solution vector are the velocities, pressures, densities, and temperatures for the gas and liquid phases. In addition, the modeling of the source term H requires special care.

Figure 5 depicts the methodology utilized to model the interfacial momentum and energy exchange.

Most analyses used today pay little attention to the interfacial momentum and energy transfer terms. In our studies, we explored the interfacial nonequilibrium modes of Richter [2] and Elias and Lellouche [3].

Source Terms

Interfacial Momentum and Energy Models

- Large Changes in Relevant Physics
 - Vapor Bubbles
 - Slug
 - Liquid Bubbles
- Interfacial Models Used
 - Combined Richter, Elias & Lellouche
- Most Codes Assume a Constant Interfacial Heat Transfer Coefficient

$$\begin{aligned} \bar{H} = & \dot{m} \\ & \text{Interfacial_Force}_x \\ & \text{Interfacial_Force}_y \\ & \text{Interfacial_Force}_z \\ & \dot{m}h_g + \text{Interfacial_Energy_Transfer} \\ & S_k \\ & S_\varepsilon \end{aligned}$$

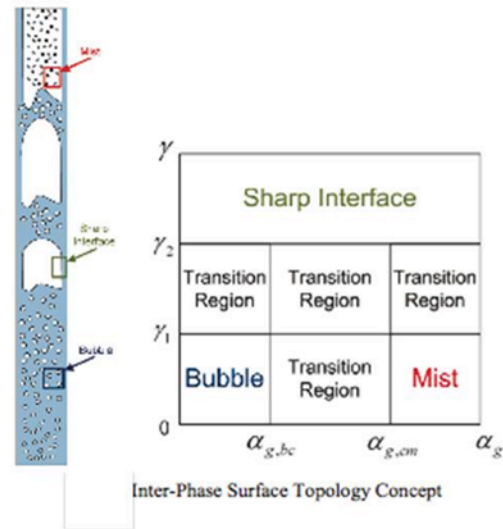
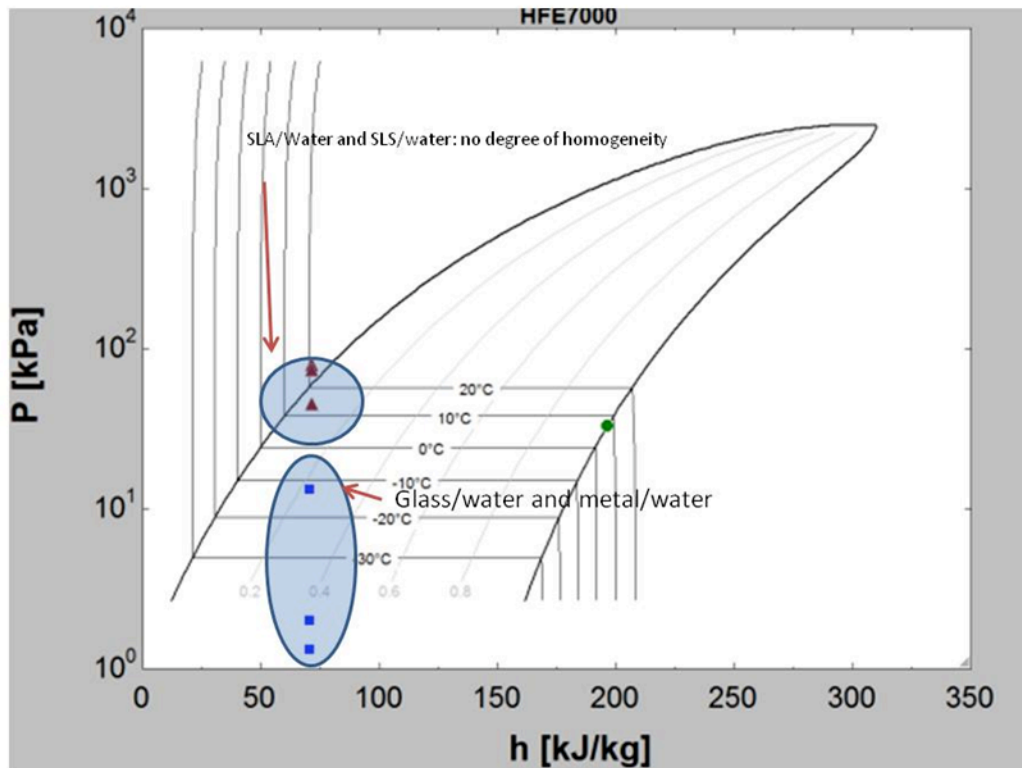


Figure 5. Source term models.

From Figure 5, one can see that a “constant” interfacial energy and momentum transfer coefficient is not reasonable. Figure 6 depicts the impact of reducing the heterogeneity of the nucleation process. Isothermal depressurization tests were conducted on rapid prototype, metal, and glass surfaces. The rapid prototype surfaces included a porous SLS and a smoother SLA material. The results of the depressurization studies were overlaid on the p-h diagram from the working refrigerant. (HFE 7000) From Figures 7 and 8, one can observe the interfacial topologies for heterogeneous- and homogeneous-type nucleation.

Performance of the Caitin cycle is also linked to how far below the saturation line we can drive the fluid in Steps 1 to 2 (see Figure 2) The key to driving down into the metastable regime is the suppression of heterogeneous nucleation. By decreasing surface roughness and increasing the surface energy, we can push well below the saturation line toward the spinodal point [4].

Nucleation Variability



Caitin Proprietary and Confidential

Figure 6. Nucleation variability test for SLS, SLA, metal, and glass surfaces. HFE7000 covered by a field liquid (water).

Nucleation testing clearly indicated that the SLS/SLA materials were not able to achieve lower nucleation temperatures. Heterogeneous nucleation will result in reduced depression in pressure prior to nucleation, resulting in reduced ΔT in the nozzle tube.



Figure 7. Heterogeneous nucleation, 3.16 mm copper tube, HFE 7000, 2 bar inlet pressure.



Figure 8. Reduced heterogeneity in the nucleation process, 2.7 mm glass tube, 2 bar inlet pressure.

Figures 7 and 8 depict the impact of reducing heterogeneity of the nucleation process by controlling the surface energies (metal versus glass).

4. Numerical Results

The Caitin cooling system was conceptualized and developed via CFD analyses. Star CCM+ was the primary code used for all simulations. Extensive user-defined routines were implemented to better model the refrigerant properties and the interfacial heat, mass and momentum transfer.

A requirement for the nozzle performance was cascaded down from the platform performance targets. In general, our objective is to obtain 1–3 kW per nozzle at a refrigerant flow rate less than 0.075 kg/s per tube.

An example of typical results is shown in Figures 9 and 10. Note the supersonic mixed Mach numbers in the tube and the presence of the condensation shock. Figure 10 depicts an example of the Caitin cooling system when applied to an electronics cooling application. In this case, we are simulating computer chip cooling by embedding the nozzle in a metal jacket. CPU processors would surround the nozzle, applying load directly to the tube.

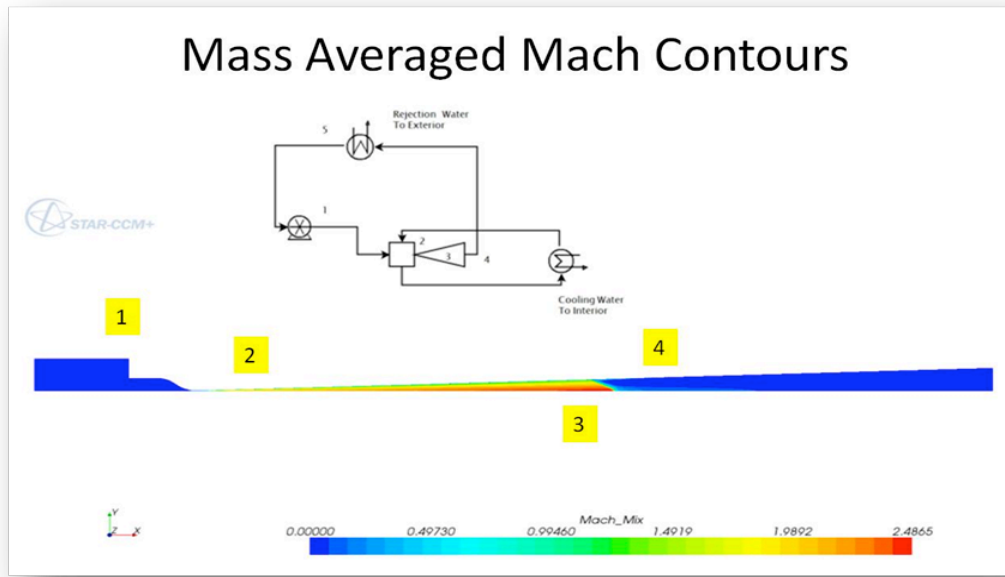


Figure 9. Mass-averaged Mach contours in Caitin cooling system nozzle.

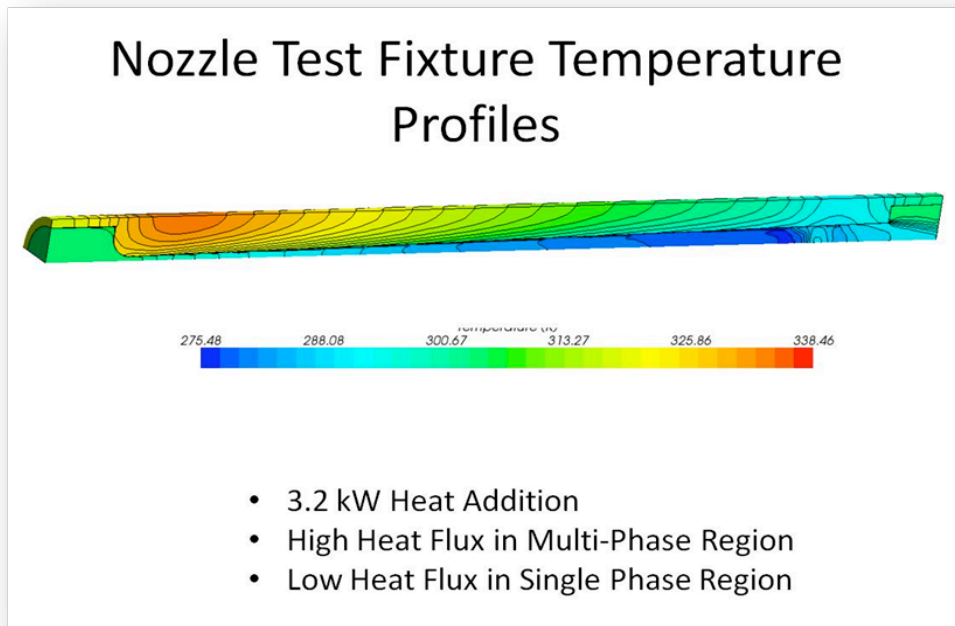


Figure 10. Temperature contours in Caitin nozzle for an electronics cooling application.

Figure 11 depicts an example of code calibration for the simulation models on our nozzles.

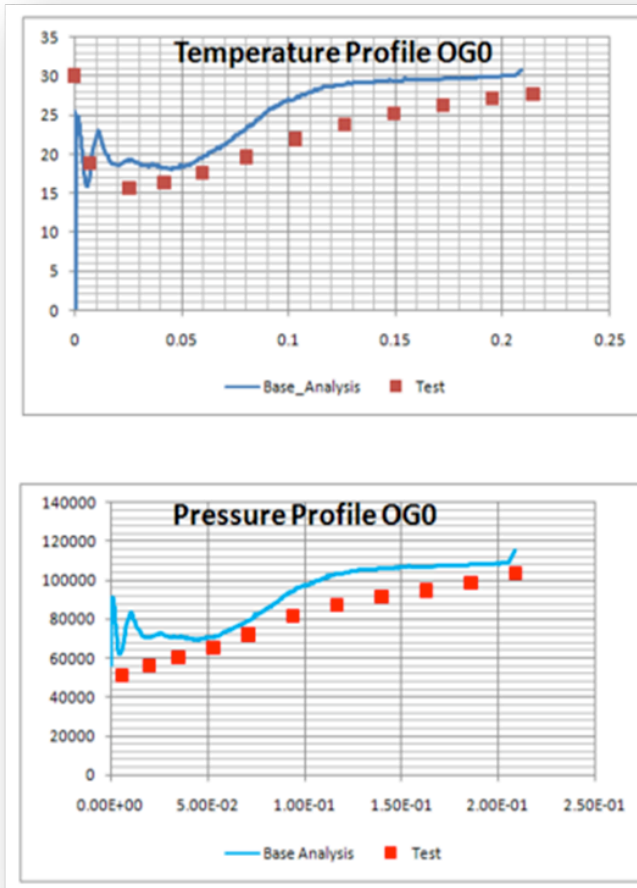


Figure 11. Simulation results for multi-nozzle interaction.

Note that the simulation results (“base analysis” on the graph) obtain reasonable accuracy but significantly differ from experiment (“test” results on the graph) in the most critical region of the nozzle—the first 10 millimeters.

From our analytical and experimental test program, we have determined that controlling the nozzle nucleation process is key to establishing good cooling performance. However, this is just the beginning of the system development. We have recently been awarded time on the Oak Ridge National Laboratory Jaguar supercomputer cluster to perform large-scale computations. The goal of these calculations will be multifaceted and include:

1. Improving the basic knowledge of the nucleation process and interfacial energy, mass, and momentum transfer process. We will accomplish this by modeling large clusters of nuclei as shown in Figures 7 and 8.
2. Performing system/platform analyses of the installed performance of the Caitin cooling system. These will include performing simulations on the complete device. The goal of these studies will be to identify system/subsystem interactions.

Example of these large-scale system problems are shown in Figures 12 and 13. Figure 12 depicts a simulation where we were studying possible nozzle-to-nozzle communication of the plumes leading to instability or unstart.

HXC Surface Temperature

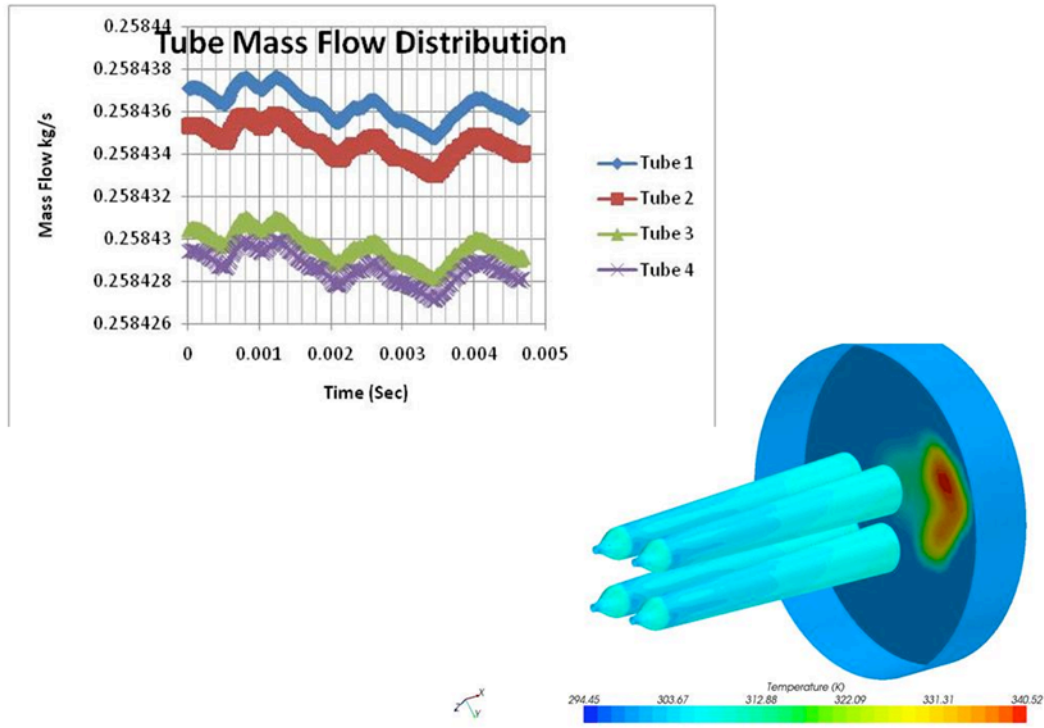


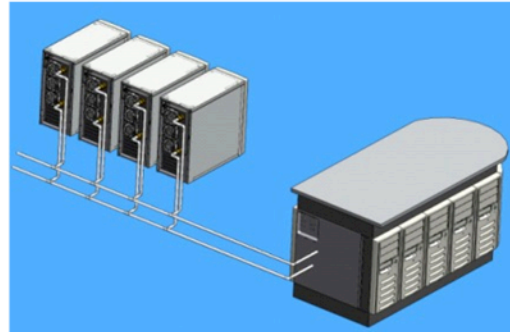
Figure 12. Simulation result for multi-nozzle interaction.

Figure 13 displays the geometric description of the Caitin cooling system. In these simulations, we will model the complete device including all heat exchangers, valves, and pumps. (Pumps may be modeled via momentum sources.)

The above simulations cannot be conducted without HPC capability. We will be running large jobs requiring massive computing power and memory.

Caitin Cooling

- Chilled Water from Caitin System, Supplied to Backplane, of Integrated Fan/Radiator Assemblies
- One Caitin System can Supply up to 15 kW of Cooling
- Caitin System Can be Integrated into Existing Cooling Systems



Caitin Cycle integrated with Backplane Cooling System

Figure 13. Caitin cooling system representation, system was configured for computer backplane cooling.

5. Summary

CAE methods have been utilized extensively in development of the Caitin cooling system. Even though the current CFD models are lacking in terms of multiphysics models, the codes can provide directional results.

Results of our simulations studies have shown that the operational flow regime, of our device, is extremely complex and in high non-equilibrium. To adequately simulate our system, we have been carrying out the following:

1. Developing computer resources inside and outside of Caitin. We have recently been awarded CPU time on the ORNL Jaguar cluster to perform high-fidelity, non-equilibrium vaporization/condensation studies.

2. Working closely with the CFD code providers (Star CCM+ and Open FOAM) to implement more accurate interfacial mass, momentum, and energy transfer models.
3. Developing a large database of experimental data that can be used for product development as well as code calibration.

Caitin has embarked on a virtual product development process, coupled with a strong experimental program. The combination of experiment and strong theoretical understanding, enabled by high-fidelity multiphysics modeling will lead to more robust product design and a reduced time to market for our system.

References

1. Moran, M. J., and Shapiro H. N., "Fundamentals of Engineering Thermodynamics," Wiley, 2000.
2. Richter, H. J., "Separated Two-Phase Flow Model: Application to Critical Two-Phase Flow," Int. J. Multiphase Flow, Vol. 9 (5), pp. 511-530, 1983.
3. Elias, E., and Lellouche, G. S., "Two-Phase Critical Flow," Int. J. of Multiphase Flow, Vol. 20, pp. 91-168, 1994.
4. DeBenedetti, P.G., Metastable Liquids, Concepts and Principles, Princeton University Press, 1996.